Modeling and Experimental Verification of a Continuous Curvature-based Soft Growing Manipulator

Justin Allen[1], Ryan Dorosh[1], Chris Ninatanta[1], Andrew Allen[1], Linlin Shui[2], Kyle Yoshida[1], Jiecai Luo[3], *Member, IEEE*, and Ming Luo[1], *Member, IEEE*

***Abstract*—Soft robots show significant potential for use in search and rescue, human-robot interaction, and other emerging fields due to their ability to easily conform, deform, and interact with their environment. However, precise control of these soft robots is still being explored. In this paper, we investigate a potential solution to address the limitations of precise control for soft robots. We experimentally verify the accuracy of a general analytical formulation of a continuous kinematic model using a custom soft growing manipulator. Next, we provide an experimental verification of its inverse kinematic model. With this precise model, most soft continuum kinematic models, whether tendon-driven or with a payload, can be represented. Our robot fits the proposed generalized curvature function for $n = 2$, with an average error relative to the robot's overall length of 5.01%, based on four robot lengths of 0.5 m, 0.8 m, 1.0 m, and 1.2 m. The inverse kinematic model was verified using three positions, resulting in errors of 2.91%, 7.91%, and 2.14%. We also showed that the shape can be recovered based on using the tip position in the inverse kinematic model. Our future work will involve verifying this model in 3D space and incorporating it into a model-based feedback loop controller to enhance position control accuracy.**

***Index Terms*—Modeling, Control, and Learning for Soft Robots; Tendon/Wire Mechanism; Continuous Curvature; Experimental Verification.**

I. Introduction

SOFT manipulators, composed of compliant materials and deformable bodies, offer an intrinsically safer alternative to rigid robots. Their extended range of flexibility coupled with an adaptable shape makes them advantageous for human-robot collaboration in complex environments and other emerging fields [1].

Nevertheless, achieving precise control of a soft robot is challenging due to its complex nonlinear material properties and limited control input bandwidth (e.g., pneumatic valves). To enhance control accuracy, it is essential to employ a kinematic model that accurately represents the manipulator's position. Currently, the most prevalent kinematic model for soft continuum robots is the constant curvature model [2]. With a pneumatic-driven steering approach, the constant curvature-based model is appropriate, since the force from pressure is uniformly distributed on the surface, resulting in a consistent curvature shape [3]. However, when considering the tendon-driven approach, a moment is generated at the tip, making the continuous curvature model more preferable [4] [5]. When an external force (e.g., payload) is applied to the end effector, causing significant bending of the soft body, both pneumatic and tendon-driven steering approaches favor a continuous curvature model [6]. In general, there are two modeling approaches related to the continuous curvature model. One option is the piece-wise constant curvature model, which divides the entire robot body into small pieces of constant curvature arcs [7] [8]. In this model, the curvature value is treated as a function of length, and this approach is commonly employed in most multi-segmented soft robots [9] [10]. The other approach

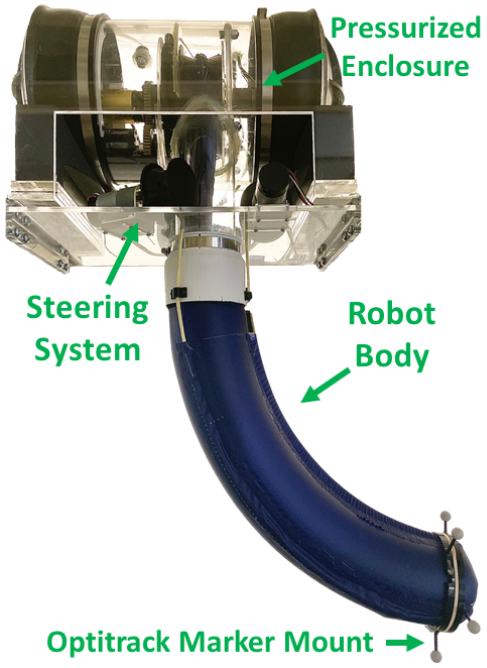

Fig. 1: Overview of the soft growing manipulator including the robot body, pressurized enclosure, steering system, and Optitrack marker mount.

Manuscript received: October, 25, 2023; Revised January, 16, 2024; February, 7, 2024.

This paper was recommended for publication by Editor Yong-Lae Park upon evaluation of the Associate Editor and Reviewers' comments.

[1]J. Allen, R. Dorosh, C. Ninatanta, A. Allen, K. Yoshida and M. Luo are with School of Mechanical and Materials Engineering, Washington State University, Pullman, WA 99163, USA Corresponding Author: ming.luo@wsu.edu

[2]L. Shui is with School of Animation and Digital Media Arts, Communication University of China, Peking, 100024, China.

[3]J. Luo is with Electrical Engineering Department, Southern University and A&M College, Baton Rouge, LA 70807, USA.

Digital Object Identifier (DOI): see top of this page.

utilizes the general formulation of the continuous curvature model, with the curvature rate being a constant with respect to the order of the length [11] [12]. Another approach for determining the kinematic model of a soft robot is through the use of inflated beam theory. This model relies on an iterative approach for solving tip position and curvature of the soft robot body [13].

In this paper, we perform a system identification on our customized single-segment soft growing manipulator's generalized continuous curvature model in a 2D plane. To assess the model's accuracy, we collected positional and angle data at the manipulator's tip rather than capturing the entire body shape [14]. The tip data not only describes the tip position and orientation in the workspace but also enables us to use our continuous curvature model to construct the theoretical robot shape. The structure of the paper is as follows: Section I provides the driving motivation and necessary background. Section II gives a brief overview of the robot and its behavior during steering. Section III delivers a generalized kinematic model and inverse kinematic (IK) approximation. Section IV describes the model verification for both the kinematic and IK model through experimental results along with a justification for our proposed model. Lastly, Section V summarizes the work presented in this paper and presents an outlook on future work with the robot.

In general, the novelties of this paper include:

1) An experimental verification of the general continuous curvature model using a custom soft growing robot.
2) An experiment showing that the model can predict tip position and angle with minimal error, allowing for simplified shape control in the future based only on information at the tip.

II. Robot Platform

Figure 1 shows the soft growing manipulator used for model verification, constructed using principles similar to other soft growing robots [15] [16] [17]. This robot exhibits the capability to extend and retract through the eversion and inversion of the fabric body. The principle of eversion has been widely discussed in other works and will not be a focus of this paper [18] [19]. The fabric body's tail is attached to a cable, which in turn links to a central motor. This robot features a fabric body constructed from silicone-coated ripstop nylon. The symmetric cross-angle of the fabric enables the robot body to expand when pressurized and curve gracefully instead of buckling when steered [20]. Steering with this robot is achieved through tendon-driven control, facilitated by three evenly spaced fabric pockets located 120° apart on the robot's body, each containing a 2.9 mm Kevlar rope. At the tip of the robot, an internal crawler is employed both for clamping the steering cables and for attaching various end-effectors using roller magnets, as described in [19] [21]. For instance, passive IR markers can be positioned on the manipulator's tip to collect positional data. When the steering cable is pulled by the gear motor, the resulting force causes the side of the internal crawler to move, leading to curvature in the robot's soft body. A simplified model of our robot is depicted in Fig. 2, which uses a spring model to illustrate the concept.

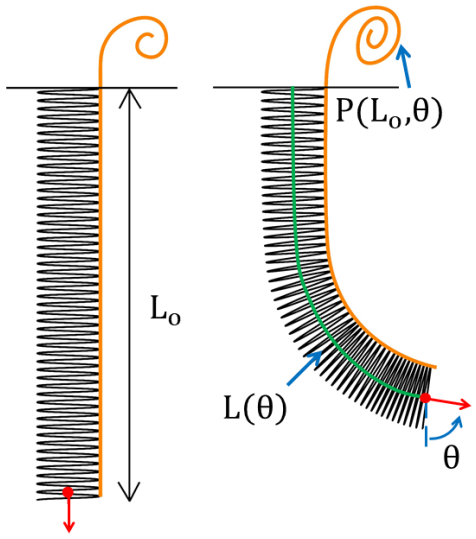

Fig. 2: Manipulator modeled as an untensioned spring at 0°. As the tip angle increases, the spring compresses and the length of the robot shortens.

When the soft growing robot is pressurized, it behaves similarly to a compression spring, with stiffness determined by the input pressure. As the steering cable is pulled, the spring begins to bend and shorten, resulting in a shape that approximates continuous curvature instead of constant curvature. It is important to note that if excessive pulling force is applied, the spring may buckle, which is not considered in our model.

III. Continuous Curvature Kinematic Model

A. Forward Kinematic Model

For our model, we derived a generalized continuous curvature function. This function is used similarly to the angle function defined in [11]:

$$\theta(L(\theta),P(L_o,\theta)) = \frac{c \cdot L(\theta)^n}{n!} \tag{1}$$

Where,

θ: The angle of the tip.

n: The order of curvature. The constant curvature model is applicable when $n = 1$. System identification is used to determine the optimal value of n to fit the soft growing manipulator's model.

c: The rate of change of curvature otherwise known as the sharpness coefficient. A larger value of c indicates more bending of the robot. System identification is applied to determine the current sharpness during steering.

L_o: The robot's initial length.

$L(\theta)$: The length of the robot. It is important to note that the robot's length decreases as steering occurs, making the length of the robot dependent on the tip angle. System identification is employed to establish the relationship between the robot's length and the tip angle. The relationship is expressed as $L(\theta) = L_o - K_n(L_o) \cdot \theta$ where $K_n(L_o)$ which is a coefficient also determined through system identification. At a tip angle of 0°, $L(0) = L_o$.

$P(L_o,\theta)$: The amount of cable length pulled during steering by the motor. When considering the same tip angle θ, the amount of pulling is determined by the initial length of the robot, denoted as $P(L_o,\theta)$. System identification characterizes this relationship.

With the results from eq. (1), the resultant two-dimensional Cartesian coordinates, (x,y), of the tip can be determined by using the Fresnel integrals [22]:

$$x = \int_0^{L(\theta)} \cos(\theta(l))\,dl, \quad y = \int_0^{L(\theta)} \sin(\theta(l))\,dl \tag{2}$$

When the base angle is at 0°, it corresponds to the point $(0,-L_o)$, after a rotation of 90°. If the robot's kinematic model aligns with the provided model, it suggests the presence of a unique tip angle, denoted as θ, and a distinct set of parameters (c, L_o, and n) for all points in the 2D space, specifically, for all values of x and y. Consequently, by knowing only the position (x,y) and the angle θ of the tip in relation to model parameter n, it becomes possible to reconstruct the entire shape without needing to capture the entire body through sensing verified in section IV-C.

B. Inverse Kinematic (IK) Model

Regarding the IK problem, which involves determining the robot's shape based on a given tip position in Cartesian coordinates, (x,y), the challenge lies in the fact that solving eq. (2) inversely can be a difficult and cumbersome process when $n \geq 2$. Instead, we opted to linearize the entire kinematic model using Taylor series approximations and then integrating to find the approximate position (x_l,y_l).

$$P_m = \sum_{i=0}^{\infty} (-1)^i \cdot \frac{c^m \cdot L(\theta)^{m\cdot n+1}}{(n!)^m \cdot (m!) \cdot (m\cdot n+1)} \tag{3}$$

(x_l,y_l) is related to the P_m above, and where

$$x_l : m = 2i+1$$
$$y_l : m = 2i$$

The variable i dictates the order of the Taylor series expansion, while m determines whether the expansion is of a sine or cosine function, resulting in either position x_l or y_l. Equation (3) can then be implemented into a genetic algorithm that minimizes the error in the x and y coordinates.

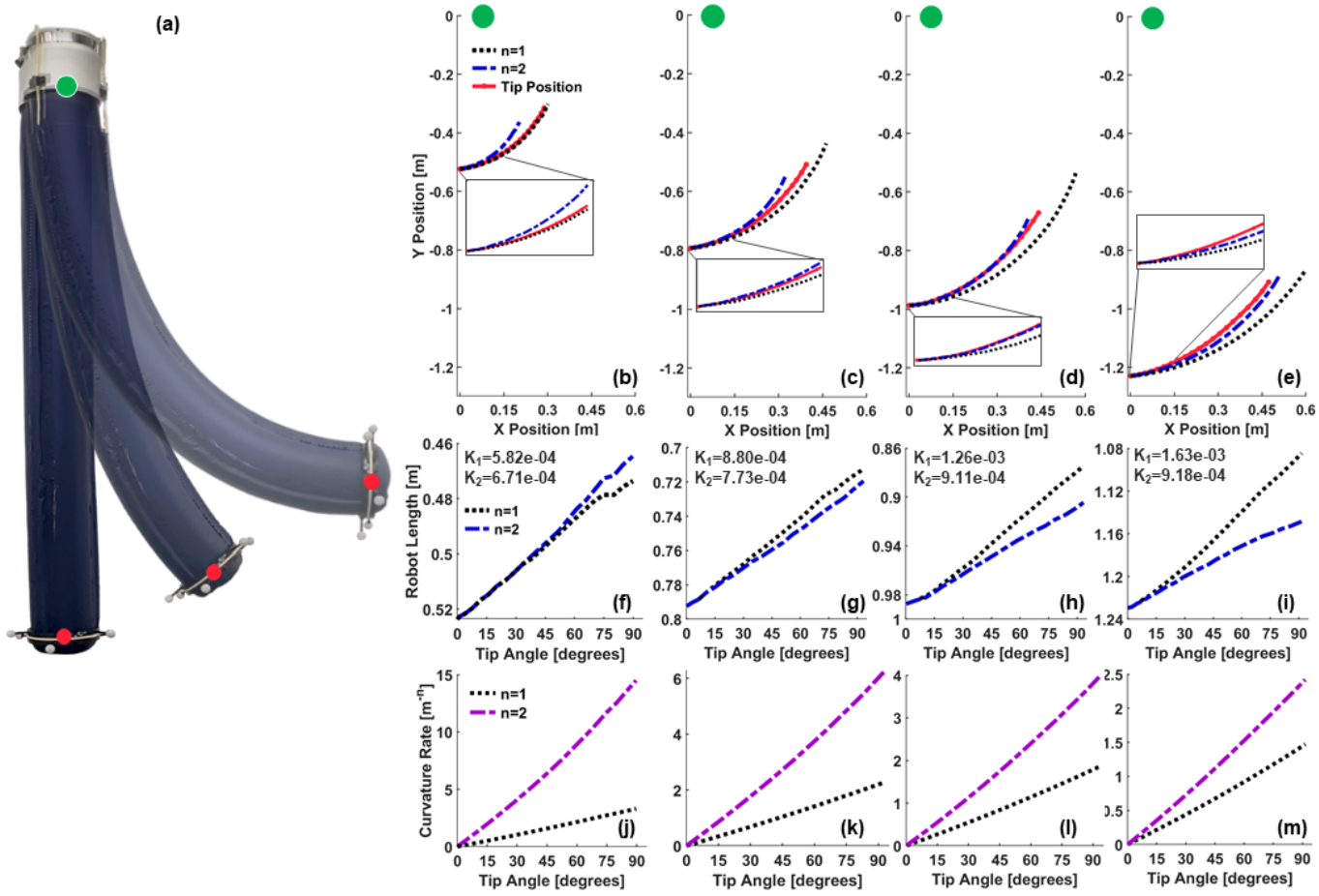

Fig. 3: (a) Robot at length of 0.8 m steering from 0° to 90°. Plots (b)-(m) show the kinematic model experimental verification results: Plots (b)-(e) show the comparison between tip position during static steering with optimal results. A zoomed-in feature highlights the area from 0 m to 0.15 m. The plots show that $n=1$ has the best fit at the shortest length (0.5 m) and that $n=2$ fits the other lengths best. Plots (f)-(i) display the model's linear decrease in length, L, with respect to tip angle, θ, as given by the slope $K_n(L_o)$. The plots (j)-(m) convey the correlation of curvature rate with respect to order n to the tip angle, which is a linear relationship.

The algorithm outputs the robot's initial length L_o and the amount of steering cable pulled $P(L_o, \theta)$, allowing the robot to reach the desired position [23].

IV. Experimental Results

A. Experimental Setup

The experimental setup for data collection involves using an Optitrack motion capture system to track the tip's position and orientation at a rate of 120 Hz, along with a Data Acquisition toolbox from US Digital to record the position of the steering motor. To simplify the overall experiment, only one steering cable is actuated to achieve pure 2D planar bending, and the input pressure is kept constant at 1.88 psi (13.0 kPa) to eliminate any influence from pressure. The maximum robot length was recorded at 1.23 m.

B. Model Verification

To ascertain whether the kinematic model (eq. (1), (2)) aligns with the robot's curved shape, data for static tip positions in four different length groups of 0.5 m, 0.8 m, 1.0 m, and 1.2 m along with tip angles ranging from 0° to 90° by pulling on the steering cable was collected. These lengths were chosen as they cover the majority of the robots workspace.

The results from this process are displayed in Fig. 3. Each group consists of twenty sets of tip positions and angles. Subsequently, the kinematic model's parameters are determined, and the error between the model-predicted tip position and the experimental position is compared. The critical steps for the search algorithm are detailed as follows:

1) The observation reveals that the robot's length decreases as the tip angle increases, therefore, the length of the next node has a larger angle θ but will possess a length that is smaller than that of the current node in the searching algorithm.
2) The tip angle θ serves as the ground truth within the search algorithm, where the error arises from the disparity between the simulated and experimental positions at the same θ.
3) The power of n ranges from 1 to 5 in the searching algorithm.

Figure 3 (b)-(m) displays the optimal results of the comparison between the model predictions and experimental data, including the visual representation of the tip position matching (x, y), the robot's length, L, decreasing as the tip angle, θ, increases, and the curvature rate, c, as a function of the tip angle during steering. Table I shows the quantitative results of the model fit based on the error percentage of overall length. To determine this percentage, the model prediction is calculated such that the position shares the same angle as the experimental data. From this, the squared Euclidean distance for a given tip angle is computed. All data points are averaged, followed by taking the square root and dividing the result by the initial length to obtain a normalized percentage. With these errors kept within a suitable range, there is an expectation that a future controller would be capable of handling any remaining compensation.

TABLE I: Error percentage of overall robot lengths based on $n = 1, 2, 3$ in the kinematic model experimental verification. The bolded error is the minimum percent error with respect to each length.

L_o	$n = 1$	$n = 2$	$n = 3$
0.526 m	**2.88%**	10.2%	16.5%
0.792 m	8.85%	**5.00%**	11.7%
0.987 m	12.7%	**1.42%**	7.89%
1.23 m	16.5%	**3.42%**	3.50%

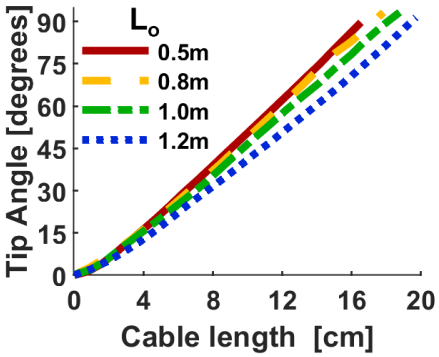

Fig. 4: Cable length pulled by gear motor based on varying initial lengths L_o in the kinematic model experimental verification.

1) The experimental data confirms that as the tip angle increases, the robot's length decreases, and this relationship appears to be linear and influenced by the initial length. In the model, $K_2(L_o)$ represents the linear relationship between $L(\theta)$ and θ when $n = 2$. We believe that this factor can be influenced by the amount of internal pressure. An increased pressure level results in a stiffer robot body, potentially causing less shortening during steering. This will be confirmed in future research.
2) It is observed that longer robot bodies require a greater amount of pulled cable length to achieve the same tip angle, as shown in Fig. 4. The amount of cable length pulled $P(L_o, \theta)$ can be calculated by eq. (4). The quadratic represents the rate of change between cable length and θ.

$$P(L_o, \theta) = (-1.079 \cdot L_o^2 + 0.640 \cdot L_o + 5.576) \cdot \theta \quad (4)$$

This factor may also be influenced by the input pressure level, which will be confirmed in future research.
3) At the shortest length (0.52 m), the best fitting result is achieved with $n = 1$, which corresponds to a constant curvature model because the tip moment generated by the steering cable does not create a significant uneven force distribution due to its short length. For a robot length of 0.79 m, the smallest error is 5.00% corresponding to $n = 2$ while $n = 1$ had a percent error of 8.85% as indicated by Table I. These higher-than-normal, yet comparable errors can be attributed to the region where the model transitions from favoring an order of $n = 1$ to $n = 2$. A second-order continuous curvature model ($n = 2$) provides a better fit for the

three longer lengths. Furthermore, a larger tip bending angle results in a greater steady-state error, as the model predicted tip position tends to underestimate the actual tip position at relatively shorter lengths. However, when steering at extended lengths, the experimental tip position transitions from being below the model prediction to surpassing it as seen in Fig. 3(b)-(e). This discrepancy can be attributed to the untwisting motion of the robot that occurs after pressurization due to fabrication bias (uneven gluing of the robot body). The fabric behavior is similar to a McKibben muscle [24]. Thus, ideally, the fabric material should be orientated at a 45° angle with respect to the longitudinal axis. However, misalignment results in an unfavorable twisting motion as seen in Fig. 6(a). This bias shortens the length, which is not accounted for in the model. Generally, $n = 2$ of the model can best represent the robot's static steering behavior.

C. Inverse Kinematic Model Verification

After determining all the parameter values of the model, the verification of the IK model is conducted as follows: We select three random points (x_r, y_r), and input them into the IK Model ($n = 2$) discussed in Section III-B. This allows us to obtain the model's output, which includes the initial length L_r and P_r, which would be the desired motor angle for the central motor controller and steering motor controller. Subsequently, both the manipulator and the amount of pulling cables are adjusted to match the desired lengths, followed by a comparison between the actual tip position and angles, represented by x, y, and θ, and the target positions, which are x_r, y_r, and θ_r. In general, this is an open loop control system without feedback (tip's position), so our goal is to verify the IK model accuracy, which could be used as a feedforward term in the future feedback loop controller design to achieve faster response with less overshoot [15]. Please note that as the model indicates the existence of only one tip angle for any given position, there is no need to specify the tip's angle, θ_r, separately as it can be determined by the model. The genetic searching algorithm is as follows:

Genetic Algorithm: A searching algorithm for determining the initial length and tip angle from tip position (x_r, y_r)

Input: (x_r, y_r)

Objective Function: Minimizing L_o, θ

Dependent Variables: c, K

Initial Values: L_j, θ_j

Constraints:

$$\sqrt{x_r^2 + y_r^2} \leq L_o \leq 2\sqrt{x_r^2 + y_r^2}$$
$$0^\circ \leq \theta \leq 90^\circ$$

Nonlinear Constraints (from Eq. 3):

$$L_o - K \cdot \theta \geq 0$$
$$|x_l - x_r, y_l - y_r| = [0, 0]$$

As aforementioned in Section III-B, finding the inverse of the Fresnel integrals is a challenging task. To circumvent this problem, a genetic algorithm was programmed in MATLAB using the global optimization toolbox. The input for the algorithm is the desired position in 2D planar space. Next, an objective function was created with the goal of minimizing the initial length and tip angle. The rate of change of curvature is computed based on eq. (1), while the slope, $K(L_o)$, is determined based on a polynomial fit using system identification. An initial estimate for the robot's length L_j, and angle, θ_j, serves as the starting point for the algorithm. To reduce computation time, the initial robot length is constrained within a range from the Euclidean distance between the robot base and desired point in space to twice that distance, while the angle is bounded between 0° and 90°. The first listed nonlinear constraint equation guarantees that the robot's length remains a positive value, in addition to defining the length denoted as $L(\theta)$. To facilitate error minimization, a linearization of the kinematic model, as represented in eq. (3) is employed to reduce the disparity between the linearized coordinates and the target position to 0. In the linearization, the Taylor series expansion was approximated to the fifth order $(i = 4)$. The algorithm completes its execution when a suitable initial length, L_r, and tip angle, θ_r, are found, and the amount of pulled cable length for steering, P_r, is then determined from eq. (4).

In Fig. 5, we present the results of our experimental verification of the IK model from three randomly selected points. The output from the IK model for these points was the robot's initial length and angle the steering motors need to rotate P_r, both of which are depicted in the figure. The position error, otherwise known as the Euclidean distance error of Fig. 5(a), was 3.212 cm. This particular point had the shortest robot length and only steered to approximately a 45° angle. In contrast, Fig. 5(b) illustrates a larger steady-state error, with a position error of 8.596 cm. This result aligns with the experimental verification data shown in Fig. 3, indicating that at larger tip angles there is a greater offset between the model-predicted position and the actual position. The last random point displayed in Fig. 5(c) had a position error of 3.547 cm and exhibited the longest robot length and the longest amount of settling time. This experimental verification provides compelling evidence that this model is a good fit for the robot. Please note: This paper primarily focuses on the static response, and it is worth noting that all motor controllers may not be optimized for performance due to the additional damping introduced by the soft manipulator body. Consequently, the dynamic response may exhibit less overshoot with the implementation of more advanced controllers. Our primary objective is to ensure that each motor reaches and stabilizes at the desired position as predicted by the IK model, and subsequently records the robot's static pose.

The shape of the robot can be estimated based on the current tip position, illustrated in Fig. 6(b)-(d). The robot's initial length was randomly selected and steered through three random points along its trajectory. These points were input into the genetic algorithm. The resultant output comprised of the tip angle and initial length are then directly used to

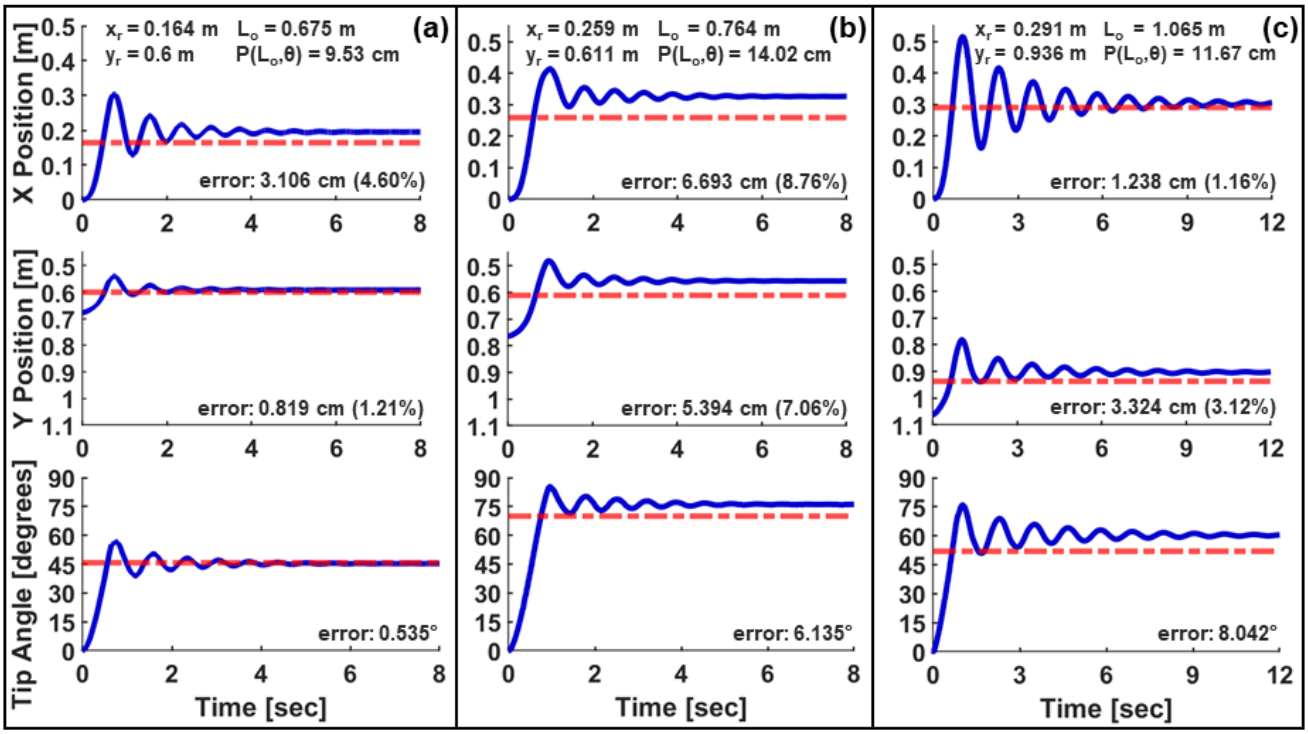

Fig. 5: Inverse kinematic (IK) model experimental verification results: (a), (b), and (c) display the dynamic responses for the robot tip's X position, Y position, and angle from the IK model's output $P(L_o, \theta)$ when provided with three different random points denoted as (x_r, y_r). Each plot also showcases the steady-state error and error percentage of overall length, serving as an illustration of the effectiveness of the IK model in the absence of a feedback controller.

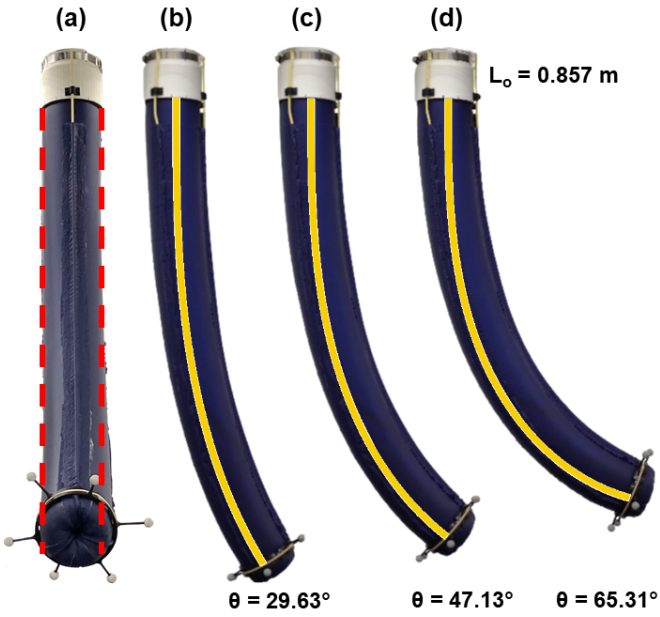

Fig. 6: Shape estimation of robot with an initial length L_o of 0.857 m. (a) Robot front view at a tip angle of 65.31°, dashed red lines depict twisting motion during steering. Images (b)-(d) illustrate the approximate shape at three different tip angles based on the kinematic model.

calculate the sharpness coefficient, c. Knowing the sharpness coefficient allows for a straightforward recovery of the robot's shape. This is achieved by incrementally varying the tip angle θ from 0° to the output tip angle from the genetic algorithm, which then determines the length at each angle using eq. (1). When comparing the IK model to the actual tip position, it was found that the maximum positional error for all three points was within the range of ≤ 1 mm. However, the difference in tip angles was notably larger, with errors of 2.18°, 4.90°, and 9.09° respectively. At lower tip angles, the disparity between the actual and estimated tip angles is smaller, so the theoretical robot shape based on the model matches closer to the center line of the robot. As the tip angle increases, the shape of the robot becomes less accurate. The generalized continuous curvature model offers a simplified approach for estimating the robot shape as shown in Fig. 6(b)-(d). This qualitative observation presents evidence that the model can provide a useful approximation of the robot's shape in an obstacle-free workspace.

D. Justification of Model

While other models such as piece-wise constant curvature would be appropriate for modeling the single-segment robot presented in this work, the model provided aims to be a generalized approach to any continuous curvature robot. The parameters in our model include two constants: the initial length L_o of the robot and the order of curvature rate n. The bending amount can be represented by various curvature rates c. Meanwhile, the piece-wise constant curvature approach requires determining the appropriate segment resolution and the curvature value for each segment, making it more complex than our model.

The polynomial curvature model that was presented in [11] uses a series of monomials that form a polynomial to

describe the robot shape. Rather than utilizing the outlined curvature function, our model is designed with the minimal number of parameters required for a generalized representation. Therefore, we found that a single monomial represented by our continuous curvature model is sufficient for accurately describing the robot's tip position and constructing the robot shape. In addition, the polynomial model was exclusively applied in a simulated environment, whereas we validated our model on an actual robotic platform.

V. Conclusion and Future Work

In this paper, we demonstrate the experimental verification of a general continuous kinematic model based on our custom soft growing manipulator using static data. The verification indicates that when $n = 2$, where the power of the curvature rate is related to the robot body's length, it represents the optimal kinematic model for our manipulator. This finding validates the hypothesis that the robot's length decreases as it steers increasingly and further underscores that tip information is sufficient to reconstruct the entire robot's shape without the need to capture data from the entire body. Additionally, we implement the inverse kinematic model and validate its accuracy through experiments.

Future work involves expanding this model into 3D-space, incorporating the input pressure as a factor, and implementing a feedback loop control system, which entails integrating the model's output as a feedforward term. A significant challenge in controller design will be addressing the reduction of steady-state errors between the desired position and the model output. This challenge arises due to the independence of the length and steering controllers, and it will require finding an effective way to coordinate and integrate these two controllers. In addition, as mentioned in section IV-C, the future controller design not only strives to guide the robot to reach the desired position but also aims to reduce the oscillation caused by the low inertia of the soft robot body. With a robust model and implementation of a controller, we seek to perform pick-and-place tasks to prepare the low-cost, safe, easily fabricated robot for use in agriculture, medical assistance, and search and rescue applications.

References

[1] J. Jørgensen, K. Borup Bojesen, and E. Jochum, "Is a soft robot more "natural"?: Exploring the perception of soft robotics in human-robot interaction," *International Journal of Social Robotics*, vol. 14, pp. 95–113, 2021.

[2] I. Robert J. Webster and B. A. Jones, "Design and kinematic modeling of constant curvature continuum robots: A review," *The International Journal of Robotics Research*, vol. 29, no. 13, pp. 1661–1683, 2010.

[3] J. D. Greer, T. K. Morimoto, A. M. Okamura, and E. W. Hawkes, "A soft, steerable continuum robot that grows via tip extension," *Soft Robotics*, vol. 6, no. 1, pp. 95–108, 2019.

[4] D. B. Camarillo, C. F. Milne, C. R. Carlson, M. R. Zinn, and J. K. Salisbury, "Mechanics modeling of tendon-driven continuum manipulators," *IEEE Transactions on Robotics*, vol. 24, no. 6, pp. 1262–1273, 2008.

[5] M. Srivastava, J. Ammons, A. B. Peerzada, V. N. Krovi, P. Rangaraju, and I. D. Walker, "3d printing of concrete with a continuum robot hose using variable curvature kinematics," in *International Conference on Robotics and Automation (ICRA)*, 2022, pp. 3216–3222.

[6] X. Huang, J. Zou, and G. Gu, "Kinematic modeling and control of variable curvature soft continuum robots," *IEEE/ASME Transactions on Mechatronics*, vol. 26, no. 6, pp. 3175–3185, 2021.

[7] P. Rao, Q. Peyron, and J. Burgner-Kahrs, "Using euler curves to model continuum robots," in *IEEE International Conference on Robotics and Automation (ICRA)*, 2021, pp. 1402–1408.

[8] T. Mahl, A. E. Mayer, A. Hildebrandt, and O. Sawodny, "A variable curvature modeling approach for kinematic control of continuum manipulators," in *American Control Conference*, 2013, pp. 4945–4950.

[9] R. K. Katzschmann, C. D. Santina, Y. Toshimitsu, A. Bicchi, and D. Rus, "Dynamic motion control of multi-segment soft robots using piecewise constant curvature matched with an augmented rigid body model," in *IEEE International Conference on Soft Robotics (RoboSoft)*, 2019, pp. 454–461.

[10] A. S. Lafmejani, H. Farivarnejad, A. Doroudchi, and S. Berman, "A consensus strategy for decentralized kinematic control of multi-segment soft continuum robots," in *American Control Conference (ACC)*, 2020, pp. 909–916.

[11] C. D. Santina and D. Rus, "Control oriented modeling of soft robots: The polynomial curvature case," *IEEE Robotics and Automation Letters*, vol. 5, no. 2, pp. 290–298, 2020.

[12] Y. Chen, Y. Cai, J. Zheng, and D. Thalmann, "Accurate and efficient approximation of clothoids using bézier curves for path planning," *IEEE Transactions on Robotics*, vol. 33, no. 5, pp. 1242–1247, 2017.

[13] J. Hwee, A. Lewis, A. Raines, and B. Hannaford, "Kinematic modeling of a soft everting robot from inflated beam theory," in *2023 IEEE International Conference on Soft Robotics (RoboSoft)*, 2023, pp. 1–6.

[14] Y. Toshimitsu, K. W. Wong, T. Buchner, and R. Katzschmann, "Sopra: Fabrication and dynamical modeling of a scalable soft continuum robotic arm with integrated proprioceptive sensing," in *IEEE/RSJ International Conference on Intelligent Robots and Systems (IROS)*, 2021, pp. 653–660.

[15] R. Dorosh, J. Allen, Z. He, C. Ninatanta, J. Coleman, J. Spieker, E. Tuck, J. Kurtz, Q. Zhang, M. D. Whiting, J. Luo, M. Karkee, and M. Luo, "Design, modeling, and control of a low-cost and rapid response soft-growing manipulator for orchard operations," in *IEEE/RSJ International Conference on Intelligent Robots and Systems (IROS)*, 2023, pp. 4184–4190.

[16] P. A. der Maur, B. Djambazi, Y. Haberthür, P. Hörmann, A. Kübler, M. Lustenberger, S. Sigrist, O. Vigen, J. Förster, F. Achermann, E. Hampp, R. K. Katzschmann, and R. Siegwart, "Roboa: Construction and evaluation of a steerable vine robot for search and rescue applications," in *IEEE 4th International Conference on Soft Robotics (RoboSoft)*, 2021, pp. 15–20.

[17] M. M. Coad, L. H. Blumenschein, S. Cutler, J. A. R. Zepeda, N. D. Naclerio, H. El-Hussieny, U. Mehmood, J.-H. Ryu, E. W. Hawkes, and A. M. Okamura, "Vine robots," *IEEE Robotics and Automation Magazine*, vol. 27, no. 3, pp. 120–132, 2020.

[18] F. Przybylski, Y. Adagolodjo, A. Mîra, G. Cerruti, J. Dequidt, C. Duriez, and P. Berthet-Rayne, "3d kinematics and quasi-statics of a growing robot eversion," in *2023 IEEE International Conference on Soft Robotics (RoboSoft)*, 2023, pp. 1–6.

[19] S.-G. Jeong, M. M. Coad, L. H. Blumenschein, M. Luo, U. Mehmood, J. H. Kim, A. M. Okamura, and J.-H. Ryu, "A tip mount for transporting sensors and tools using soft growing robots," in *2020 IEEE/RSJ International Conference on Intelligent Robots and Systems (IROS)*, 2020, pp. 8781–8788.

[20] D. A. Haggerty, M. J. Banks, E. Kamenar, A. B. Cao, P. C. Curtis, I. Mezić, and E. W. Hawkes, "Control of soft robots with inertial dynamics," *Science Robotics*, vol. 8, no. 81, p. eadd6864, 2023.

[21] C. Ninatanta, R. Cole, I. Wells, A. Ramos, J. Pilgrim, J. Benedict, and R. Taylor, "Design and evaluation of a lightweight soft electrical apple harvesting gripper," in *IEEE International Conference on Soft Robotics (RoboSoft)*, 2023.

[22] A. Lekkas, A. R. Dahl, M. Breivik, and T. Fossen, "Continuous-curvature path generation using fermat's spiral," *Modeling, Identification and Control (MIC)*, vol. 34, pp. 183–198, 10 2013.

[23] M. Luo, E. H. Skorina, W. Tao, F. Chen, and C. D. Onal, "Optimized design of a rigid kinematic module for antagonistic soft actuation," in *IEEE International Conference on Technologies for Practical Robot Applications (TePRA)*, 2015, pp. 1–6.

[24] K. T. Yoshida, X. Ren, L. H. Blumenschein, A. M. Okamura, and M. Luo, "Afrees: Active fiber reinforced elastomeric enclosures," in *IEEE International Conference on Soft Robotics*. IEEE, 2020, pp. 305–311.